Non-Darcy and radiative effects on convective embankment modeling

Marc Lebeau & Jean-Marie Konrad
Department of Civil and Water Engineering – Laval University
Quebec, QC, Canada

GEOQuébec 2015
Challenges from North to South
Des défis du Nord au Sud

ABSTRACT
The design of convective embankments generally hinges on the use of numerical models that describe buoyancy-driven flow and heat transfer in porous media. A review of the literature reveals that most of the models used in the study of convective embankments assume that heat transfer occurs by conduction and convection, and that airflow can be described with Darcy's law. This is inconsistent with recent experimental evidence that suggests that radiative heat transfer is significant, and that Darcy's law does not apply to rockfill materials. In response to these shortcomings, a new model is herein derived to account for both radiative heat transfer and non-Darcy effects. Once validated, the model is used to gain insight into the relative importance of radiative heat transfer and non-Darcy flow on the thermal response of a typical railway embankment. The radiative heat transfer is shown to be greater during the summer months. This increases the temperature at the base of the embankment, which in turn, increases the wintertime convective heat transfer. This additional heat extraction does not counteract the effect of the radiative heat transfer, and the wintertime temperatures below the embankment are shown to be warmer than that computed without radiative and non-Darcy effects.

RÉSUMÉ
La conception des remblais convectifs s'effectue généralement avec des modèles numériques qui décrivent le transfert de masse et de chaleur en milieu poreux. Une revue de la littérature révèle que la plupart des modèles considèrent que le transfert de chaleur s'effectue par conduction et convection, et que le transfert de masse peut être décrit avec la loi de Darcy. Cette approche est contraire aux résultats d'études expérimentales récentes qui démontrent que le transfert de chaleur par radiation est important, et que la loi de Darcy ne s'applique pas aux matériaux d'enrochements. En réponse à ces lacunes, l'article présente un nouveau modèle qui tient compte du transfert de chaleur par radiation et des effets non Darcien. Le modèle est utilisé afin d'établir les effets de l'écoulement transitionnel et du transfert de chaleur par radiation sur le comportement thermique d'un remblai de chemin de fer typique. Il est démontré que le transfert de chaleur par radiation augmente la température à la base du remblai en période estivale, ce qui intensifie le transfert de chaleur par convection en période hivernale. Cette extraction de chaleur supplémentaire s'avère toutefois insuffisante pour contrer l'apport de chaleur par radiation et les températures hivernales à la base du remblai sont plus élevées que celles calculées sans effets radiatifs et non Darcien.

1 INTRODUCTION

The growing necessity for natural resources has prompted a renewed interest in Arctic and sub-Arctic regions, and led to the development of new transportation corridors. The design of the transportation lines within these corridors is challenged by the presence of permafrost, which is sensitive to minor changes in heat transfer at the ground surface. Overlooking the effect of these manmade structures on the surface heat balance can result in significant thaw, and settlement, of the underlying permafrost. Over the years, a number of techniques have been proposed to mitigate the effect of embankment construction on thaw settlement. These techniques include the use of air ducts, thermosyphons, and convective embankments that enhance wintertime heat extraction. In this latter technique, the embankments are specifically engineered to enhance the wintertime heat extraction that occurs as convection currents cool the underlying permafrost. The design of these convective embankments unavoidably hinges on our understanding of buoyancy-driven flow and heat transfer in coarse-grained porous media. This knowledge has been integrated into a number of numerical models for studying the behavior of convective embankments in permafrost-laden regions of Canada (Arenson et al. 2006; Lebeau and Konrad 2009; Fredlund and Zhang 2012), China (Lai et al. 2003; Sun et al. 2009; Pei et al. 2014; Zhang et al. 2005), and the United States of America (Goering and Kumar 1996, 1999; Goering 2003). All of these models assume that heat transfer occurs by conduction and convection, and most consider that airflow can be described with Darcy's law. This is inconsistent with recent experimental evidence that suggests that radiative heat transfer is significant, and that Darcy's law does not adequately describe the relation between superficial flux and gradient in coarse-grained soils. More precisely, Fillion et al. (2011) determined the effective (combined conductive and radiative) thermal conductivity of four samples of crushed-rock with effective particle diameters ranging from 0.09 to 0.15 m. The effective thermal conductivity at ambient temperatures was found to be 97 to 209% greater than that ascribed to heat conduction. The effective thermal conductivity was also shown to increase with increasing effective particle diameter. Zhang et al. (2013), on the other hand, determined the airflow characteristics of four samples of crushed-rock with effective particle diameters ranging from 0.07 to 0.22 m. The tests were conducted in a wind tunnel, and yielded nonlinear relations between the superficial flux and gradient. These relations were shown to conform to the Darcy-Forchheimer law, which accounts for both viscous and inertial effects.

In response to these shortcomings, the paper proposes a new model for studying the behaviour of convective embankments that accounts for both non-Darcy and radiative effects. Once validated, the model is used to establish the importance of non-Darcy flow and radiative heat transfer on the response of a typical railway embankment.

2 NUMERICAL MODEL

2.1 Theory

The general mechanisms through which heat is transferred in convective embankments are conduction, convection, radiation, and phase changes. Heat conduction occurs as hot, rapidly moving or vibrating atoms and molecules transfer their energy to neighbouring particles. It may also involve a rearrangement of water hydrogen bonds. Heat convection, on the other hand, occurs as pore fluid moves within the porous media. More precisely, forced convection results from the movement of pore fluid caused by pressure differences whereas natural convection, or buoyancy-driven flow, results from the tendency of most fluids to experience changes in density with variations in temperature, pressure, and composition. These changes in density interact with the gravity vector to produce fluid motion. Hence, as a given mass of fluid is heated, it expands and becomes less dense and thus, more buoyant than the surrounding fluid. This causes the heated fluid to rise above the colder surrounding fluid. Heat radiation occurs as electromagnetic waves propagate across pore-air spaces. In the case of phase changes, a characteristic amount of energy is absorbed or released by the fluid as it transitions from one state to another.

The mathematical description of these processes hinges on the combination of the principle of mass and energy conservation, the equation of state of the fluid, and phenomenological equations describing heat conduction, heat radiation, and fluid flow in porous media. The resulting partial differential equations differ according to the form of these components and the use of simplifying assumptions. It is herein assumed that the various constituents of the porous media are in local thermal equilibrium and thus, that the temperature of the constituents is the same within a representative elementary volume. In addition, the pore air is considered to be a gray, emitting, and absorbing medium in which radiation travels only a short distance before being absorbed. In this case, each soil particle is subjected only to the radiation emitted by its neighbours, and the radiative heat transfer can be expressed as a diffusion equation. Under these assumptions, the heat transfer equation results from the insertion of Fourier's law and the radiative diffusion equation into the equation of energy conservation for a cubic volume of porous media with soil-water phase change, from liquid to solid, or vice versa. Mostly concerned with the movement of pore air, the pore water is herein assumed immobile. The mass transfer equation for pore air results from inserting the Darcy-Forchheimer law into the equation of mass conservation for a cubic volume of porous media. The Oberbeck-Boussinesq approximation is considered valid in the range of expected temperatures, pressures, and compositions. It is thus assumed that viscous dissipation is negligible, and that pore-air properties other than density remain constant. Although the pore-air is considered thermally compressible, its density is treated as constant everywhere except in the gravity term of the momentum equation. The Oberbeck-Boussinesq approximation also implies that the equation of state can be linearized around reference density $\rho_{a,o}\left(u_{a,o},T_o\right)$ where $u_{a,o}$ and T_o are the reference pore-air pressure and absolute temperature, respectively. These assumptions result in the following equations for non-Darcy convective and radiative heat transfer in isotropic porous media:

$$\text{Heat:}\quad \vec{\nabla}\cdot\left[k_t^e\,\vec{\nabla}T\right]=C_t^a\frac{\partial T}{\partial t}+C_{t,a}\vec{q}_a\cdot\vec{\nabla}T$$

$$\text{Mass:}\quad \vec{\nabla}\cdot\left[\frac{\tilde{K}}{\mu_{a,o}}\vec{\nabla}\left(u_a+\rho_a\vec{g}z\right)\right]=0 \qquad [1]$$

$$\text{State:}\quad \rho_a=\rho_{a,o}\left[1-\beta_o\left(T-T_o\right)\right]$$

where C_t is the volumetric heat capacity of the soil at constant pressure, $C_{t,a}$ is the volumetric heat capacity of air at constant pressure, $C_t^a=C_t+L_f\,\partial\theta_w/\partial T$ is the apparent volumetric heat capacity of the soil, $\vec{g}$ is the gravity vector, $\tilde{K}$ is the apparent intrinsic permeability, $k_t^e=k_t^c+k_t^r$ is the effective thermal conductivity, k_t^c is the conductive component of effective thermal conductivity, k_t^r is the radiative component of effective thermal conductivity, L_f is the volumetric latent heat of fusion of water, $\vec{q}_a=-\tilde{K}/\mu_{a,o}\,\vec{\nabla}\left(u_a+\rho_a\vec{g}z\right)$ is the volumetric flux vector of air, t is the time, T is the absolute temperature, u_a is the pore-air pressure, x,z are the spatial coordinates, β_o is the reference volumetric thermal expansion coefficient of air, θ_w is the volumetric fraction of liquid water, $\mu_{a,o}$ is the reference dynamic viscosity of air, and ρ_a is the density of air. It must be emphasized that these equations are very similar to those found for laminar convective heat transfer in porous media (Lebeau and Konrad 2009). The difference essentially lies in the constitutive relations used to describe soil permeability and thermal conductivity.

2.2 Constitutive relations

2.2.1 Water freezing function

The relation between the volumetric fraction of liquid water and temperature is often referred to as the water freezing function. As highlighted above, the first derivative of this function with respect to temperature forms an integral part of the apparent volumetric heat capacity term. Although the actual shape of the function has very little effect on computed temperatures, it must allow for an exact computation of the change in volumetric enthalpy over a specific temperature range. In order to meet this requirement, the water freezing function is herein expressed as follows (Mottaghy and Rath 2005):

$$q_w = \begin{cases} \left(q_{w,u} - q_{w,f}\right) e^{-\left(\frac{T - T_L}{w}\right)^2} + q_{w,f} & T < T_L \\ q_{w,u} & T \geq T_L \end{cases} \qquad [2]$$

where $w » \left(T_L - T_S\right)/2$ is a curve shape parameter, T_L is the fusion (liquidus) temperature, T_S is the solidification (solidus) temperature, and $q_{w,f}, q_{w,u}$ are the volumetric fractions of liquid water in the frozen and unfrozen soil, respectively. This form of equation is also used to describe the conductive component of effective thermal conductivity and volumetric heat capacity of the soil.

2.2.2 Radiative component of thermal conductivity

The radiative component of thermal conductivity depends on the transparency, or penetrability to electromagnetic waves, of the different constituents of the porous medium. In the case of transparent constituents, the electromagnetic waves pass through the medium without any radiative heat transfer. In contrast, the electromagnetic waves will be absorbed at the surface of a medium with completely opaque constituents. Gray, or optically thick, constituents provide an intermediate response by allowing for short-range transmission of thermal radiation. In the case of a continuous medium, with similar gray absorbing-emitting and non-scattering constituents, the integral form of the radiative heat transfer equation can be converted into the following diffusion equation (Siegel and Howell 1992):

$$\vec{q}_r = -\frac{4\sigma}{3\alpha_R}\vec{\nabla} T^4 \qquad [3]$$

where $\vec{q}_r$ is the radiative heat flux vector, a_R is the Rosseland mean absorption coefficient, and s is the Stefan-Boltzmann constant. Assuming that the polynomial temperature function can be linearized around T_o such that $T^4 = 4T_o^3 T - 3T_o^4$, the diffusion equation reduces to

$$\vec{q}_r = -\frac{16\sigma T_o^3}{3\alpha_R}\vec{\nabla} T \qquad [4]$$

or, then again

$$\vec{q}_r = -k_t^r \vec{\nabla} T \qquad [5]$$

where $k_t^r = \left(16 s T_o^3\right)/\left(3 a_R\right)$ is the radiative component of effective thermal conductivity. This equation was originally derived by Rosseland (1936) and is often referred to as the Rosseland, or diffusion, approximation. Yet, it must be noted that the solid particles are generally opaque and that the radiative heat transfer only takes place within the voids of the porous medium. In this case, the radiative heat transfer can be considered as a local effect that occurs between the surfaces of neighbouring particles. For the sake of simplicity, let us consider a gray fluid confined between two infinite isothermal parallel plates of opaque material with gray-diffuse surfaces. In this simple geometrical arrangement, the expression for radiative heat flux is found by applying Oppenheim's (1956) electrical network analogy for heat exchange between diffuse gray bodies (Lienhard and Lienhard 2011):

$$q_r = -\frac{s}{\frac{1}{e_1} + \frac{1}{e_2} - 1}\left(T_2^4 - T_1^4\right) \qquad [6]$$

where e_1, e_2 and T_1, T_2 are the emissivity and absolute temperature of the different surfaces, respectively. Multiplying the numerator and denominator by the plate separation distance, which is herein set equal to the particle diameter, and simplifying the temperature function such that $T_2^4 - T_1^4 = \left(T_2^2 + T_1^2\right)\left(T_2 + T_1\right)\left(T_2 - T_1\right) \simeq 4\bar{T}^3\left(T_2 - T_1\right)$ where $\bar{T} = \frac{(T_2 + T_1)}{2}$, yields

$$q_r = -\frac{4 D s \bar{T}^3}{\frac{1}{e_1} + \frac{1}{e_2} - 1}\frac{¶T}{¶x} \qquad [7]$$

For plates with similar surface emissivity, the equation reduces to

$$q_r = -4\left(\frac{e}{2 - e}\right) D s \bar{T}^3 \frac{\partial T}{\partial x} \qquad [8]$$

This equation has often been used to describe the radiative heat flux between particle surfaces in discontinuous, or discrete models, which treat the porous medium as an assembly of units, or cells, of idealized geometry (Argo and Smith 1953; Beveridge and Haughey 1971). A number of similar equations have also been derived for differently shaped surfaces (Wakao and Kato 1969). Although quite accurate, the discontinuous models are often criticized for neglecting the effect of long-range radiation that propagates through the voids of the porous medium. The pseudo-continuous model circumvents this limitation by representing the porous medium as a random assembly of solid particles, and solving the radiative heat transfer equation as if the medium were a continuum. In the case of a parallel-plane layer of absorbing, emitting, and scattering medium, the expression for radiative heat flux is found by applying Hamaker's (1947) extension of the Schuster-Schwarzschild approximation (Chen and Churchill 1963):

$$q_r = -4\left[\frac{2}{(a+2b)D}\right]D\bar{T}^3\frac{\partial T}{\partial x} \qquad [9]$$

where a and b are the absorption and scattering coefficients, respectively. Given that the medium is treated as a continuum, these coefficients are not directly related to physical properties such as porosity and particle surface emissivity. Although these coefficients can be determined experimentally, Vortmeyer (1978) established a theoretical relation between the pseudo-continuous and discontinuous models that leads to specific expressions for parameters a and b. Using these expressions yields

$$q_r = -4\left[\frac{e}{(2-e)}+\frac{2L}{(2-e)(1-L)}\right]Ds\bar{T}^3\frac{\partial T}{\partial x} \qquad [10]$$

where L is the long-range radiation transmission parameter, which is a function of porosity and particle surface emissivity (Vortmeyer and Börner 1966). As expected, this equation reduces to equation [8] as the long-range radiation parameter approaches zero. A number of studies have shown that this equation provides acceptable predictions of radiative heat flux in the absence of conduction and convection (Vortmeyer 1978). Hence, unless otherwise stated, the radiative component of thermal conductivity is herein expressed as follows

$$k_t^r = 4\left[\frac{e}{(2-e)}+\frac{2L}{(2-e)(1-L)}\right]Ds\bar{T}^3 \qquad [11]$$

It must be noted that Fillion et al. (2011) have shown that the long-range radiation parameter can be set equal to zero in predictions of the effective (combined conduction and radiation) thermal conductivity of crushed-rock samples.

2.2.3 Apparent intrinsic permeability

Darcy's law is the simplest model for describing airflow in porous media. Initially derived from empirical evidence, the law states that the superficial flux is a linear function of the potential energy gradient, such that

$$\vec{\nabla}\left(u_a+\rho_a\vec{g}z\right) = -\frac{\mu_{a,o}}{K}\vec{q}_a \qquad [12]$$

where K is the intrinsic permeability. Unfortunately, this linear function is only valid at small values of superficial flux. At larger fluxes, the form drag due to solid particles increases, and the linearity transitions into a nonlinear relation. In this non-Darcy flow, the appropriate form of the momentum equation reads as follows (Joseph et al. 1982):

$$\vec{\nabla}\left(u_a+\rho_a\vec{g}z\right) = -\frac{\mu_{a,o}}{K}\vec{q}_a - \frac{c_F\rho_a\left|\vec{q}_a\right|}{\sqrt{K}}\vec{q}_a \qquad [13]$$

where $\left|\ \right|$ is the Euclidean norm, and c_F is the dimensionless form-drag constant. The first term on the right-hand side of this equation is Darcy's viscous term whereas the second term is Forchheimer's inertial term. The nonlinear nature of this equation can be relegated to the permeability term by rearranging the equation as follows

$$\vec{q}_a = -\frac{K}{\mu_{a,o}\left(1+\dfrac{\sqrt{K}c_F\rho_a\left|\vec{q}_a\right|}{\mu_{a,o}}\right)}\vec{\nabla}\left(u_a+\rho_a\vec{g}z\right) \qquad [14]$$

or, then again

$$\vec{q}_a = -\frac{\tilde{K}}{\mu_{a,o}}\vec{\nabla}\left(u_a+\rho_a\vec{g}z\right) \qquad [15]$$

where $\tilde{K} = K\Big/\left(1+\frac{\sqrt{K}c_F\rho_a\left|\vec{q}_a\right|}{\mu_{a,o}}\right)$ is the apparent intrinsic permeability. The flux-dependent apparent intrinsic permeability can be substituted by a potential energy gradient dependence by introducing the flux equation into the expression for the apparent intrinsic permeability. In so doing, the apparent intrinsic permeability reads (Knupp and Lage 1995):

$$\tilde{K} = \frac{-1+\sqrt{1+4\dfrac{K^{3/2}c_F\rho_a\left|\vec{\nabla}\left(u_a+\rho_a\vec{g}z\right)\right|}{\mu_{a,o}^2}}}{2\dfrac{\sqrt{K}c_F\rho_a\left|\vec{\nabla}\left(u_a+\rho_a\vec{g}z\right)\right|}{\mu_{a,o}^2}} \qquad [16]$$

Although the expression may seem daunting, it is of great practical importance as it expresses the nonlinear character of the flow in terms of the independent variable.

3 NUMERICAL SOLUTION

The equations for non-Darcy convective and radiative heat transfer are solved with a script-driven partial differential equation solver called FlexPDE (PDE Solutions Inc. 2011). The solver performs the operations needed to turn the partial differential equations, domain, and auxiliary definitions into a Galerkin finite element model. The working principle of the solver consists in assigning trial values of the independent variables to each node of the quadratic order triangular elements. These values are then substituted into the partial differential equations. At this point, the differential equations are not exactly satisfied, and errors appear at different points within the computational domain. These errors are then multiplied by weighting functions, and integrated over the triangular elements using Gaussian quadrature. This process is repeated until the trial values minimize the error in each integral. In nonlinear time-dependent problems, a single modified Newton-Raphson step is taken at each time-step while an adaptive procedure measures the solution curvature in time, and adapts the time step to maintain accuracy. An adaptive mesh refinement procedure also measures the accuracy of the integrals, and locally refines the mesh until a user-defined tolerance is achieved. The solver also allows for additional grid refinement criteria. This is particularly useful in the apparent heat capacity formulation of soil-water phase change in which a pre-generated fixed mesh generally results in an unrealistic oscillatory progression of the freezing, or thawing, front. In this study, the triangular elements are split if the nodal temperature spans a range greater than $\left[-w/2, w/2\right]$ around $\left(T_L + T_S\right)/2$.

4 CONVECTIVE EMBANKMENT MODELLING

The construction of surface infrastructures in cold regions inevitably alters the ground-surface energy balance. These changes, although minor, can lead to thawing and settlement of underlying permafrost with eventual failure of the surface infrastructure. The risks and costs of such failures has led to the development of specifically engineered embankments that enhance wintertime heat extraction to counteract the changes in ground-surface energy balance. Goering and Kumar (1996, 1999) and Goering (1996, 1998) were among the first to conduct research on wintertime convection in engineered embankments. This work was later followed by a comprehensive and well-documented numerical analysis of laminar convective flow in a typical railway embankment (Goering 2003). The railway embankment problem is herein revisited with specific emphasis on the effects of radiative heat transfer and non-Darcy flow.

As in the original study, the physical domain encompasses the model railway embankment and its foundation. As shown in Figure 1, the thermal boundary conditions consist of a combination of prescribed heat fluxes and temperatures. Since the upper boundaries are in contact with the environment, annual harmonic sine functions are determined with surface specific *N*-factors and air temperature conditions corresponding to those of a subarctic discontinuous permafrost zone. These temperature functions are given in Table 1, where time is in Julian days. The geothermal gradient is assumed to prevail along the lower boundary of the domain whereas centerline symmetry and negligible heat fluxes dictate that the normal component of the temperature gradient be set equal to zero on the remaining boundaries. Apart from the pervious embankment surface, the boundaries are considered impervious and the normal component of the pressure gradient is set equal to zero. Table 2 summarizes the basic engineering properties of the embankment and subgrade materials. The remaining properties are taken from the literature. For instance, Zhang et al. (2013) determined the airflow characteristics of four samples of crushed-rock with effective particle diameters ranging from 0.07 to 0.22 m. The tests were conducted in a wind tunnel, and yielded form-drag constants ranging from 0.17 to 0.21. Given the similarity of these materials with the generic rockfill of the railway embankment, the form-drag constant is herein set equal to 0.20. The emissivity of igneous, sedimentary, and metamorphic rocks can be taken equal to 0.925, 0.966, and 0.952, respectively (Salisbury and D'Aria 1992). In this study, the emissivity of the generic rockfill material is set equal to an average value of 0.942, and the long-range radiation parameter is set equal to zero.

The simulation covers a period of twenty-one (21) years, which eliminates the effect of the initial conditions. During this period, the adaptive refinement procedure resulted in unstructured meshes ranging from 719 (1530 nodes), in summertime, to 5089 (10318 nodes) in wintertime. The time-steps, on the other-hand, were largest in summer and smallest in winter. Figure 1 shows the temperature contour plots and stream traces on specific days during the final years of simulation. Specific isotherms are also highlighted and compared to those previously obtained for laminar convective flow without radiation. On July 1st, some of the stream traces are shown to enter through the toe of the embankment and travel towards the upper surface whereas the remainder of the stream traces loop through the core and exit through the embankment toe. During this period, the isotherms are closely spaced and parallel to the

Table 1. Annual harmonic temperature functions for the railway embankment problem.

	N-factor Freeze	*N*-factor Thaw	Temperature function (K)
T_a	N/A	N/A	$269.35 - 20.00 \cdot \sin\left[\frac{2 \cdot p}{365} \cdot \left(t + 82.25\right)\right]$
T_{s-1}	0.50	0.50	$271.25 - 10.00 \cdot \sin\left[\frac{2 \cdot p}{365} \cdot \left(t + 82.25\right)\right]$
T_{s-2}	0.90	1.90	$274.25 - 26.10 \cdot \sin\left[\frac{2 \cdot p}{365} \cdot \left(t + 82.25\right)\right]$

Table 2. Engineering properties for the railway embankment problem (Goering 2003).

Property		Foundation	Embankment (rockfill)
$C_{t,f}$	[MJ/(m^3·K)]	2.380	1.020
$C_{t,u}$	[MJ/(m^3·K)]	3.750	1.020
D	[m]	7.5×10^{-5}	6.3×10^{-2}
$k^c_{t,f}$	[W/(m·K)]	2.300	0.346
$k^c_{t,u}$	[W/(m·K)]	1.500	0.346
K	[m^2]	1×10^{-100}	6.3×10^{-7}
θ_a		0.000	0.350
$\theta_{w,u}$		0.649	0.000
ρ_d	[kg/m^3]	1442	1625

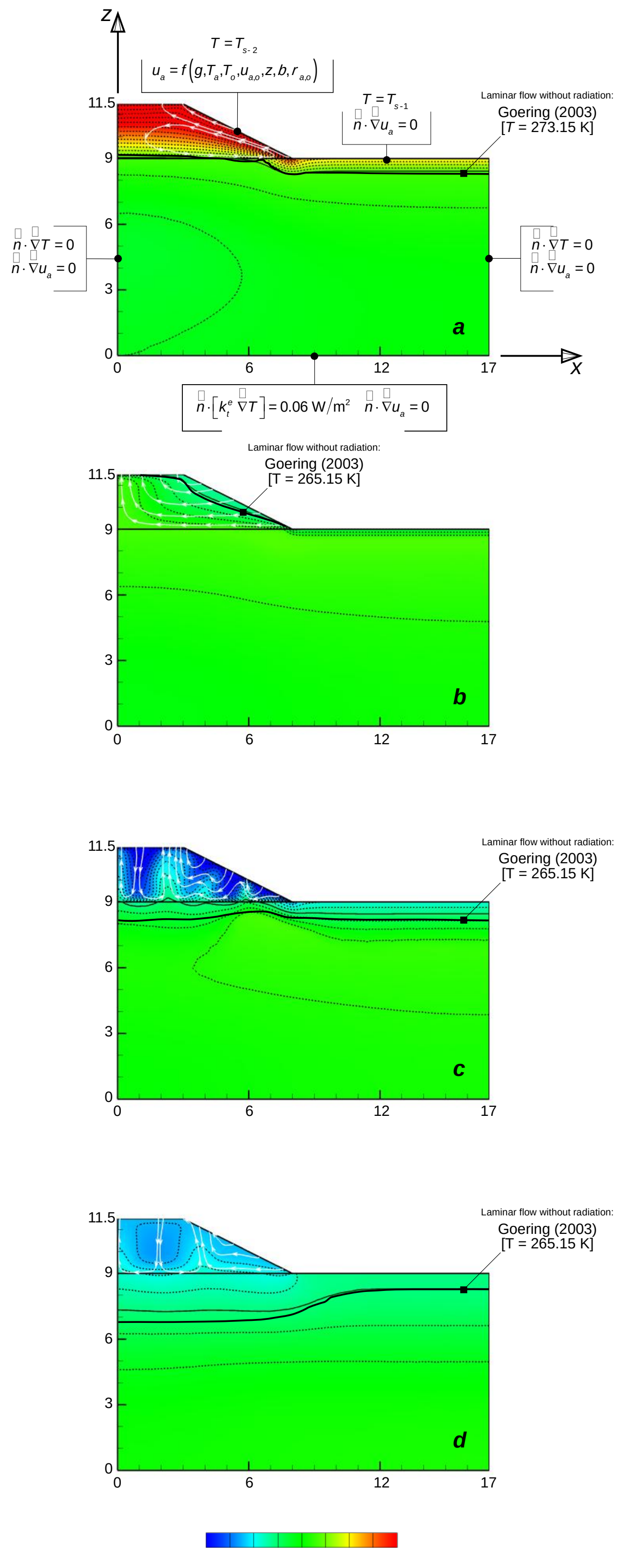

Figure 1. Temperature contour plot and stream traces for the railway embankment problem. (a) July 1st. (b) November 1st. (c) January 1st. (d) March 1st. Isotherms and stream traces are drawn in black and white, respectively.

embankment surface. This steep vertical temperature gradient suggests that heat transfer is mostly governed by conduction and radiation, with little to no effect of natural convection. A comparison of the 273.15 K isotherms reveals that the additional radiative heat transfer moves the thaw front closer towards the base of the embankment. As of November 1st, the cold ambient air enters through the side slope and ascends as it extracts heat from the core of the embankment. The shape of the isotherms is then strongly influenced by the cold boundary temperatures, and the ascending warmer pore-air. On January 1st, the stream traces form a series of convection currents that move the cold ambient air inwards and expel the warmer pore-air. This convective motion produces distinctive finger-like isotherms within the embankment. By this point, the temperature below the embankment is warmer than that obtained for laminar convective flow without radiation. As shown later in the paper, this is mostly due to the radiative heat transfer and not the effect of inertia. On March 1st, remnants of the convection currents remain, and the temperature below the embankment is much colder than that below the undisturbed surface. Once again, the temperature below the embankment is warmer than that found for laminar convective flow without radiation.

Figure 2 provides additional insight into the effects of radiative heat transfer and non-Darcy flow by plotting various model results as a function of time. As shown in Figure 2b, the mean magnitude of the pore-air fluxes within the embankment varies from a minimum of 8.2×10^{-4} m/s, on the vernal equinox (in March), to a maximum of 5.3×10^{-3} m/s, at the end of autumn (in December). This maximum value is slightly larger than that obtained for laminar convective flow without radiation. It must also be noted that the maximum value of the mean magnitude of the pore-air fluxes translates into a Reynolds number, Re, of 25. Although there is no general consensus on the threshold Reynolds number at which flow deviates from Darcy's law (Zeng and Grigg 2006), it is undeniably inferior to 25.

Figure 2c shows the mean apparent intrinsic permeability as a function of time. As expected, the mean apparent intrinsic permeability tends to decrease with increasing airflow velocity, and it tends to rise with decreasing velocities. In this case, the minimum mean apparent intrinsic permeability is found to be equal to 5.92×10^{-7} m^2, which is only 6% smaller than the stagnant intrinsic permeability. These subtle changes in intrinsic permeability should have very little effect on the convective heat transfer within the embankment.

Figure 2d shows the mean effective thermal conductivity as a function of time. The effective thermal conductivity is shown to be consistent with its mathematical formulation as it varies with the cubic power of temperature. In essence, the effective thermal conductivity decreases during wintertime and increases with warming temperatures. This inevitably leads to a greater amount of heat transfer during the warmer months. In this case, the average mean effective thermal conductivity is found to be equal to 0.60 W/(mK) with minimum and maximum values of 0.55 and 0.65 W/(mK), respectively. This average value of effective thermal conductivity is 73% greater than the thermal conductivity ascribed to heat conduction. It must be emphasized, however, that the minimum effective thermal conductivity is only 15% smaller than the maximum value.

Although the effective (combined conduction and radiation) thermal conductivity is much greater that the thermal conductivity ascribed to heat conduction, its annual fluctuations are relatively small. This results in

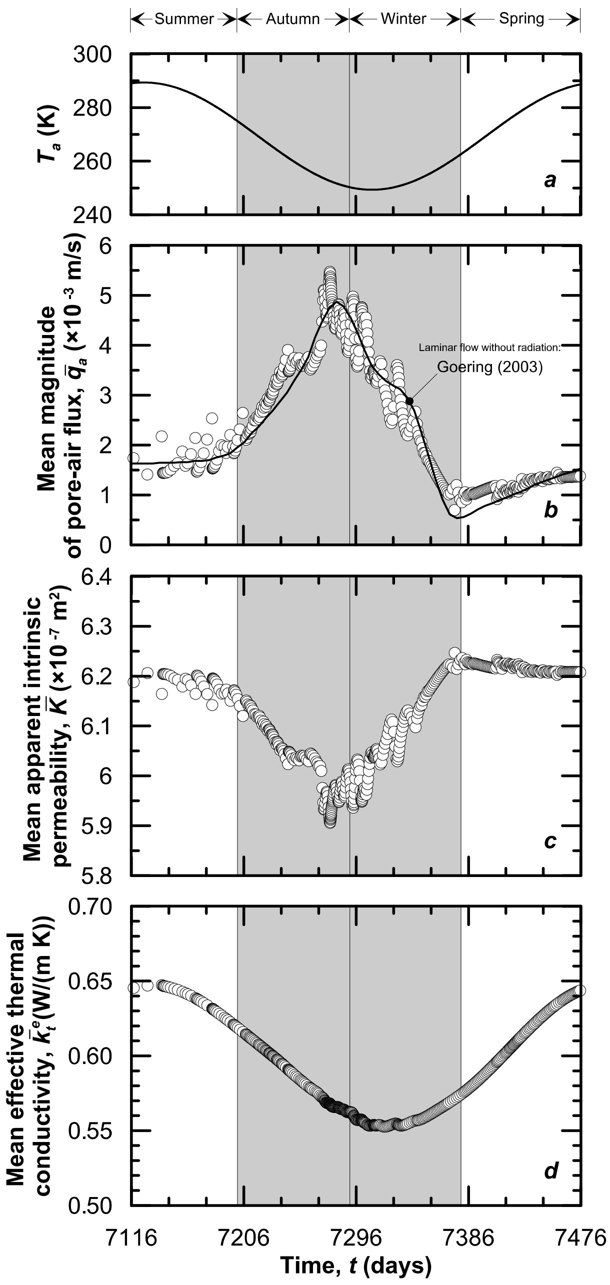

Figure 2. Annual variation of thermal and hydraulic characteristics in the railway embankment problem. (a) Ambient temperature. (b) Mean magnitude of the pore-air flux within the embankment. (c) Mean apparent intrinsic permeability of the embankment material. (d) Mean effective thermal conductivity of the embankment material.

slightly more heat input into the embankment during the summer months. As previously indicated, the additional heat transfer increases the temperature at the base of the embankment, which in turn, increases the convective motion. This supplemental convective heat extraction does not counteract the effect of the radiative heat transfer, and results in warmer temperatures below the embankment during the winter months. This effect would inevitably be compounded by greater annual temperature variations.

5 CONCLUSION

Most numerical models for studying the behavior of convective embankments have been derived for laminar convective flow. As such, these models have assumed that heat transfer occurs solely by conduction and convection, and that airflow can be described with Darcy's law. Yet, recent experimental evidence has shown that radiative heat transfer is significant, and that Darcy's law does not adequately describe airflow in rockfill materials. Motivated by these shortcomings, a new model is proposed for studying the behavior of convective embankments including non-Darcy and radiative effects. As formulated, the model accounts for most of the relevant heat transfer mechanisms, and requires very little additional computational effort. Once validated, the model was used to further our understanding of the thermal response of a typical railway embankment. In accordance with previous findings, the prime effect of non-Darcy flow was to slowdown the convection motion in regions where airflow velocity was most significant. The thermal radiation, on the other hand, was shown to be most significant during the summer months. This additional heat input increased the temperature at the base of the embankment, which in turn, increased the wintertime convective motion. This convective heat extraction was found to be insufficient to counteract the effect of the radiative heat transfer, and warmer temperatures were shown to prevail below the embankment during the winter months.

ACKNOWLEDGEMENTS

The authors gratefully acknowledge the financial support of NSERC-Hydro-Québec Industrial Research Chair for life cycle optimisation of embankment dams. The authors also extend their appreciation to their industrial partners: Hydro-Québec, SNC-Lavalin, WSP, Qualitas, AECOM, Klohn Crippen Berger, Golder Associates, and ConeTec.

REFERENCES

Arenson, L.U., Sego, D.C., and Newman, G. 2006. The use of a convective heat flow model in road designs for Northern regions. *In* EIC Climate Change Technology. pp. 1-8.

Argo, W.B., and Smith, J.M. 1953. Heat transfer in packed beds. Prediction of radial rates in gas-solid beds. Chemical Engineering Progress **49**(8): 443-451.

Beveridge, G.S.G., and Haughey, D.P. 1971. Axial heat transfer in packed beds. Stagnant beds between 20 and 750°C. International Journal of Heat and Mass Transfer **14**(8): 1093-1113.

Chen, J.C., and Churchill, S.W. 1963. Radiant heat transfer in packed beds. AIChE Journal **9**(1): 35-41.

Fillion, M.-H., Côté, J., and Konrad, J.-M. 2011. Thermal radiation and conduction properties of materials ranging from sand to rock-fill. Canadian Geotechnical Journal **48**(4): 532-542.

Fredlund, M., and Zhang, J. 2012. Benchmarks for solving coupled Thermal, Hydraulic, and Air (THA) numerical models in roadways in cold regions. *In* Cold Regions Engineering 2012. Sustainable Infrastructure Development in a Changing Cold Environment. *Edited by* G. Doré and B. Morse. American Society of Civil Engineers. pp. 326-336.

Goering, D.J. 1996. Air convection embankments for roadway construction in permafrost zones. *In* Eighth International Conference on Cold Regions Engineering. *Edited by* R.F. Carlson. American Society of Civil Engineers. pp. 1–12.

Goering, D.J. 1998. Experimental investigation of air convection embankments for permafrost-resistant roadway design. *In* Seventh International Conference on Permafrost. *Edited by* A.G. Lewkowicz and M. Allard. Centre d'études nordiques, Université Laval. pp. 319-326.

Goering, D.J. 2003. Passively cooled railway embankments for use in permafrost areas. Journal of Cold Regions Engineering **17**(3): 119-133.

Goering, D.J., and Kumar, P. 1996. Winter-time convection in open-graded embankments. Cold Regions Science and Technology **24**(1): 57-74.

Goering, D., and Kumar, P. 1999. Permeability effects on winter-time natural convection in gravel embankments. *In* Advances in Cold-Region Thermal Engineering and Sciences. *Edited by* K. Hutter, Y. Wang and H. Beer. Springer Berlin Heidelberg. pp. 455-464.

Hamaker, H.C. 1947. Radiation and heat conduction in light-scattering material. I. Reflection and transmission. Philips Research Reports **2**: 55-67.

Joseph, D.D., Nield, D.A., and Papanicolaou, G. 1982. Nonlinear equation governing flow in a saturated porous medium. Water Resources Research **18**(4): 1049-1052.

Knupp, P.M., and Lage, J.L. 1995. Generalization of the Forchheimer-extended Darcy flow model to the tensor permeability case via a variational principle. Journal of Fluid Mechanics **299**: 97-104.

Lai, Y., Li, J., Niu, F., and Yu, W. 2003. Nonlinear thermal analysis for Qing-Tibet railway embankments in cold regions. Journal of Cold Regions Engineering **17**(4): 171-184.

Lebeau, M., and Konrad, J.-M. 2009. Natural convection of compressible and incompressible gases in undeformable porous media under cold climate conditions. Computers and Geotechnics **36**(3): 435-445.

Lienhard, J.H.I., and Lienhard, J.H.V. 2011. A heat transfer textbook. 4th ed. Phlogiston Press, Cambridge, Massachusetts, USA.

Mottaghy, D., and Rath, V. 2006. Latent heat effects in subsurface heat transport modelling and their impact on palaeotemperature reconstructions. Geophysical Journal International **164**(1): 236-245.

Oppenheim, A.K. 1956. Radiation analysis by the network method. Transactions of the American Society of Mechanical Engineers. Journal of Heat Transfer **78**(4): 725-735.

PDE Solutions. 2011. FlexPDE reference manual. Spokane Valley, WA.

Pei, W., Zhang, M., Lai, Y., Jin, L., and Harbor, J. 2014. Thermal stability analysis of crushed-rock embankments on a slope in permafrost regions. Cold Regions Science and Technology **106–107**(0): 175-182.

Rosseland, S. 1936. Theoretical astrophysics. Atomic theory and the analysis of stellar atmospheres and envelopes. Clarendon Press, Oxford.

Salisbury, J.W., and D'Aria, D.M. 1992. Emissivity of terrestrial materials in the 8–14 μm atmospheric window. Remote Sensing of Environment **42**(2): 83-106.

Siegel, R., and Howell, J.R. 1992. Thermal radiation heat transfer. 3rd ed. Hemisphere Publishing Corporation, USA.

Sun, B., Yang, L., Liu, Q., Wang, W., and Xu, X. 2009. Numerical analysis for critical thickness of crushed rock revetment layer on Qinghai–Tibet Railway. Cold Regions Science and Technology **57**(2–3): 131-138.

Vortmeyer, D. 1978. Radiation in packed beds. *In* Sixth International Heat Transfer Conference. National Research Council of Canada. pp. 525-539.

Vortmeyer, D., and Börner, C.J. 1966. Die Strahlungsdurchlaßzahl in Schüttungen. Chemie Ingenieur Technik **38**(10): 1077-1079.

Wakao, N., and Kato, K. 1969. Effective thermal conductivity of packed beds. Journal of Chemical Engineering of Japan **2**(1): 24-33.

Zeng, Z., and Grigg, R. 2006. A criterion for non-Darcy flow in porous media. Transport in Porous Media **63**(1): 57-69.

Zhang, M., Lai, Y., Li, D., Chen, W., and Tong, G. 2013. Experimental study on ventilation characteristics of a concrete-sphere layer and a crushed-rock layer. International Journal of Heat and Mass Transfer **59**: 407-413.

Zhang, M., Lai, Y., Liu, Z., and Gao, Z. 2005. Nonlinear analysis for the cooling effect of Qinghai-Tibetan railway embankment with different structures in permafrost regions. Cold Regions Science and Technology **42**(3): 237-249.